Polymer 219 (2021) 123542

Contents lists available at ScienceDirect

Polymer

journal homepage: http://www.elsevier.com/locate/polymer

Inter/intramolecular hydrogen bonding mediate miscible blend formation between near-perfect alternating Poly(styrene-*alt*-hydroxyphenylmaleimide) copolymers and Poly(vinyl pyrrolidone)

Wei-Ting Du [a,1], Esam A. Orabi [b,1], Mohamed Gamal Mohamed [a,b], Shiao-Wei Kuo [a,c,*]

[a] Department of Materials and Optoelectronic Science, Center of Crystal Research, National Sun Yat-Sen University, Kaohsiung, 804, Taiwan
[b] Chemistry Department, Faculty of Science, Assiut University, Assiut, 71516, Egypt
[c] Department of Medicinal and Applied Chemistry, Kaohsiung Medical University, Kaohsiung, 807, Taiwan

ARTICLE INFO

Keywords:
Free radical copolymerization
Alternating copolymers
Hydrogen bonding interactions
Quantum chemical calculations

ABSTRACT

In this study we synthesized two isomeric hydroxyphenylmaleimide (HPMI) monomers, with *para* (*p*HPMI) or *ortho* (*o*HPMI) OH groups, and subjected them to free radical copolymerization with styrene to form the near-perfect alternating copolymers poly(S-*alt*-*p*HPMI) and poly(S-*alt*-*o*HPMI), respectively. We used nuclear magnetic resonance and Fourier transform infrared (FTIR) spectroscopy, MALDI-TOF mass spectrometry, and quantum chemical calculations to characterize the chemical structures, hydrogen bonding interactions, and alternating sequence distributions of the two HPMI-based copolymers. Poly(S-*alt*-*p*HPMI) and poly(S-*alt*-*o*HPMI) formed miscible blends with the homopolymer poly(vinyl pyrrolidone) (PVP) due to strong intermolecular hydrogen bonding between the OH groups of the copolymers and the C═O groups of PVP, as revealed from FTIR spectral analysis and quantum chemical calculations. Because the *ortho* OH groups of the phenolic units of *o*HPMI experienced additional intramolecular hydrogen bonding with the C═O groups of the maleimide units, their intermolecular interactions were limited and weaker than those of the *para* OH groups of *p*HPMI. These differences in hydrogen bonding ultimately affected the thermal properties of the copolymers and their blends with PVP.

1. Introduction

Most polymer blends are immiscible because a large molecular weight or a high degree of polymerization can result in low entropy of mixing, based on the thermodynamic viewpoint of Flory–Huggins theory [1–4]. Therefore, specific interactions (e.g., dipole–dipole or hydrogen bonding) between polymers are generally required to influence the Gibbs free energy and form miscible polymer blend systems [5–8]. The inter-association/self-association equilibrium constant ratio (K_A/K_B) of the hydrogen-bonded donor and acceptor units plays an important role in determining the phase behavior of hydrogen-bonded polymer blends, according to the Painter–Coleman association model [9–12]. The well-known nonpolar homopolymer polystyrene (PS) is immiscible with most homopolymers [e.g., poly(methyl methacrylate) (PMMA), polycaprolactone (PCL), poly(vinyl pyrrolidone) (PVP)], with the notable exceptions of poly(vinyl methyl ether) and poly(phenylene oxide) [13–17]. To improve the miscibility of PS with other polymers, various functional groups capable of intermolecular hydrogen bonding can be introduced [e.g., hydrogen bond acceptor (C═O) or donor (OH) units]. For example, the copolymer poly(styrene-*co*-vinylphenol) (PS-*co*-PVPh) displays enhanced miscibility with hydrogen-bond-accepting homopolymers [13–17]. Jiang et al. reported that a small amount of PVPh (as low as 2 mol%) improved the miscibility of PS with PMMA segments [13]. In a previous study we have shown that immiscible PS/PCL blends became miscible when PVPh was present in PS-*co*-PVPh at > 13 mol% [18]. Furthermore, when the PVPh content was >11 mol% in PS-*co*-PVPh, the immiscible PVP homopolymer became miscible with the PS-*co*-PVPh copolymer because of strong OH···O═C hydrogen bonding between the PVPh and PVP components [15]. Nevertheless, we believe that not only the concentration of PVPh

* Corresponding author. Department of Materials and Optoelectronic Science, Center of Crystal Research, National Sun Yat-Sen University, Kaohsiung, 804, Taiwan.
E-mail address: kuosw@faculty.nsysu.edu.tw (S.-W. Kuo).
[1] These authors contributed equally to this work.

https://doi.org/10.1016/j.polymer.2021.123542
Received 16 December 2020; Received in revised form 6 February 2021; Accepted 11 February 2021
Available online 17 February 2021
0032-3861/© 2021 Elsevier Ltd. All rights reserved.

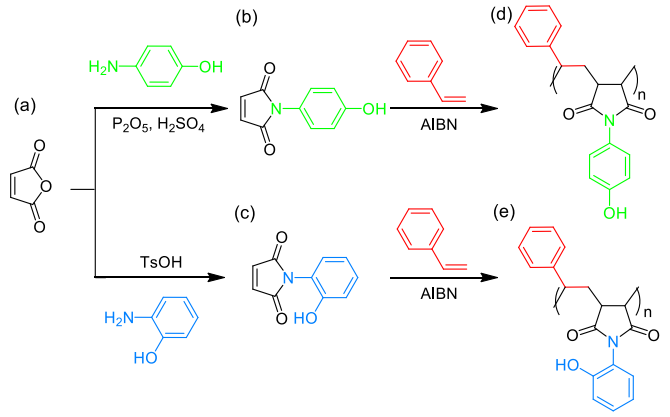

Scheme 1. Synthesis of (b) *p*HPMI and (c) *o*HPMI from the reaction of maleic anhydride (a) with *4*-aminophenol and *2*-aminophenol, and their corresponding alternating copolymerization with styrene monomer to form (d) poly(S-*alt*-*p*HPMI), and (e) poly(S-*alt*-*o*HPMI), respectively.

in PS-*co*-PVPh but also the sequence distribution of the copolymer would affect its miscibility and thermal properties when blended with other polymers capable of hydrogen bonding. In general, the vinylphenol monomer cannot undergo free radical polymerization directly because side reactions and chain transfer reactions occur to form low-molecular-weight PVPh; thus, various protected monomers [e.g., acetoxystyrene, butoxystyrene, butyldimethylsilyloxystyrene] have been used in the preparation of PVPh homopolymers or PS-*co*-PVPh copolymers [19–24]. The reactivity ratios of styrene with acetoxystyrene (r_{St} = 0.72; r_{AS} = 2.34) [19] and of styrene with butyldimethylsilyloxystyrene (r_{St} = 1.1; r_{Bsos} = 0.6) [20] result in a more random sequence distribution for PS-*co*-PVPh copolymers derived from the latter pair of monomers. A more random sequence distribution for this copolymer would significantly decrease the amount of self-association or intra-chain hydrogen bonding of the PVPh segments, because the styrene units would behave as diluent segments and decrease the value of K_B of the PVPh units, thereby increasing the K_A/K_B ratio and enhancing the miscibility. For example, we have found previously that PS-*co*-PVPh containing 16–51 mol% of PVPh was miscible with PAS [24]. Furthermore, 45–75 mol% of PVPh made the copolymer miscible with polycarbonate (PC) [25]. The repulsive interactions of the PS and PVPh segments can also enhance the large positive interaction parameter for the segments and improve the miscibility, due to a so-called "copolymer repulsion effect" [26]. Based on those previous studies, we suspected that an alternating sequence distribution of phenolic and styrene monomer units would strongly inhibit self-association or intra-chain hydrogen bonding. Poly(styrene–*alt*–maleic anhydride) (SMA) is a polymer having a well-established alternating sequence distribution, arising from the reactivity ratios of styrene with maleic anhydride being r_{St} = 0.05 and r_{MA} = 0.005 [27]. Similarly, *N*-(*p*-hydroxyphenyl)maleimide (*p*HPMI) [Scheme 1(b)] and *N*-(*o*-hydroxyphenyl)maleimide (*o*HPMI) [Scheme 1(c)] are vinyl monomers that also possess pendant phenolic functional units and can also result in alternating sequence distributions when copolymerized with styrene to form PS-*alt*-PHPMI copolymers [28,29]. PHPMI-based polymers usually possess high thermal stabilities and high glass transition temperatures (T_g) and related alternating copolymers have been used in composite matrices, toughening agents, and photoresists [28,29]. In this study we synthesized two PS-*alt*-PHPMI copolymers, in which the phenolic OH groups were located at the *para* or *ortho* positions, and then formed miscible blends of them with a PVP homopolymer through strong intermolecular hydrogen bonding between the OH groups of the PHPMIs and the C═O groups of the PVP. We chose PVP as the hydrogen-bond-accepting homopolymer because its value of K_A with the PVPh homopolymer (K_A = 6000) has been the highest ever measured for a polymer blend system featuring a single-site hydrogen bonding interaction [30–32]. In addition, the *ortho*-OH group of *o*HPMI can undergo intramolecular hydrogen bonding with the C═O groups of the maleimide moiety and, thus, the K_A/K_B ratio of its polymer should be quite different from that of the copolymer derived from the *para*-OH–containing *p*HPMI [33–35]. We synthesized our two different PS-*alt*-PHPMI copolymers, with *para* and *ortho* OH groups in the PHPMI units, through free radical copolymerization without the need for protecting groups [28,29]. We used Fourier transform infrared (FTIR) and nuclear magnetic resonance (NMR) spectroscopy, mass-analyzed laser desorption ionization time-of-flight (MALDI-TOF) mass spectrometry, and quantum chemical simulations to examine the chemical structures, hydrogen bonding interactions, and sequence distributions of these two alternating copolymers. We prepared miscible polymer blends of PVP with the two PS-*alt*-PHPMI copolymers through solution-casting and characterized them using differential scanning calorimetry (DSC), FTIR spectroscopy, and quantum chemical calculations to investigate the miscibility of and intermolecular hydrogen bonding interactions in the PS-*alt*-PHPMI/PVP blends.

2. Experimental section

2.1. Materials

2-Aminophenol (99%), maleic anhydride (98%), styrene (99%), phosphorus(V) oxide (98%), and PVP (M_n = 58,000 g/mol) were purchased from Alfa Aesar. *4*-Aminophenol (≥99%) was purchased from Sigma–Aldrich. Sulfuric acid (H_2SO_4, 96%), *N*,*N*-dimethylformamide (DMF), tetrahydrofuran (THF), methanol (MeOH), and toluene were purchased from Acros Organic and used without further purification. *p*-Toluenesulfonic acid monohydrate (*p*-TsOH·H_2O) and azobisisobutyronitrile (AIBN) were purchased from SHOWA.

2.2. N-(p-hydroxyphenyl)maleimide (pHPMI)

A solution of maleic anhydride (2.00 g, 20.4 mmol) and 4-aminophenol (2.18 g, 20.0 mmol) in DMF (12 mL) in a 100-mL three-neck round-bottom flask was stirred for 30 min in an ice bath. A solution of P_2O_5 (1.59 g, 11.2 mmol) in H_2SO_4 (1.3 mL) and DMF (9 mL) was added dropwise into the flask and then the mixture stirred for 3 h at 70 °C under N_2 atmosphere. The resulting solution was chilled in an ice bath and then cold water was poured into the flask. The precipitate was filtered off, washed with distilled water, recrystallized (2-propanol), and dried in a vacuum oven at 60 °C for 24 h to give dark yellow/green needles. Yield: 42.3%; m.p. 188 °C (Figure S1); FTIR (KBr, cm^{-1}): 1703 (C═O), 3482 (O–H); ^{1}H NMR (500 MHz, DMSO-d_6, δ, ppm): 6.83 (m, 2H, Ar**H**), 7.08 (m, 2H, Ar**H**), 7.11 (s, 2H, C**H**═C**H**), 9.72 (s, 1H, O**H**); ^{13}C NMR (125 MHz, DMSO-d_6, δ, ppm): 115.46, 122.54, 128.46 (Ar**C**), 134.56 (**C**H═**C**H), 157.06 (**C**OH), 170.36 (**C**═O). Thermal decomposition temperatures (T_{d5} and T_{d10}) were 226 and 246 °C, respectively, for *p*HPMI (Figure S2).

2.3. N-(o-hydroxyphenyl)maleimide (oHPMI)

A solution of maleic anhydride (2.00 g, 20.4 mmol) and 2-aminophenol (2.18 g, 20.0 mmol) in toluene (48 mL) and DMF (12 mL) in a 100-mL three-neck round-bottom flask was stirred for 30 min in an ice bath. A solution of *p*-TsOH·H_2O (0.500 g, 2.9 mmol) in DMF (4 mL) was added dropwise into the flask and then the mixture was heated under reflux for 12 h under N_2 atmosphere. The material was purified chromatographically (SiO_2; hexane/EtOAc, 1:1) to give a brown powder. Yield: 36.2%; m.p. 144 °C (Figure S3); FTIR (KBr, cm^{-1}): 1707 (C═O), 3377 (O–H); ^{1}H NMR (500 MHz, DMSO-d_6, δ, ppm): 6.87 (td, J = 7.5, 1.0 Hz, 1H, Ar**H**), 6.95 (dd, J = 8.0, 1.0 Hz, 1H, Ar**H**), 7.12 (dd, J = 7.5, 1.5 Hz, 1H, Ar**H**), 7.15 (s, 2H, C**H**═C**H**), 7.27 (td, J = 8.0, 1.5 Hz, 1H, Ar**H**), 9.85 (s, 1H, O**H**); ^{13}C NMR (500 MHz, DMSO-d_6, δ, ppm): 116.48, 118.61, 119.17,

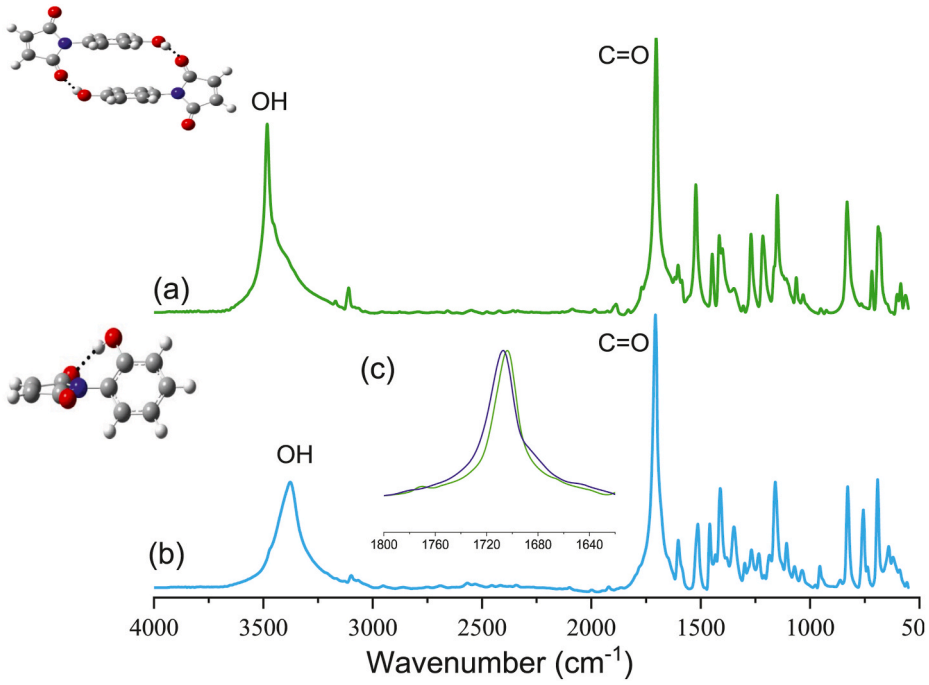

Fig. 1. FTIR spectra of (a) *p*HPMI, (b) *o*HPMI, and (c) the expansion of C═O absorptions of HPMIs.

130.26, 130.45 (Ar**C**), 135.00 (**C**H═**C**H), 154.00 (**C**OH), 170.18 (**C**═O). Thermal decomposition temperatures (T_{d5} and T_{d10}) were 223 and 240 °C, respectively, for *o*HPMI (Figure S4).

2.4. Poly(S-alt-pHPMI) and poly(S-alt-oHPMI) alternating copolymers

A solution of *p*HPMI or *o*HPMI (0.750 g, 4.00 mmol), styrene (0.41 g, 4.00 mmol), and AIBN (5 wt%) in dry THF (25 mL) in a 50-mL three-necked round-bottom flask was stirred under N_2 atmosphere at 70 °C for 24 h. The reaction was quenched by exposing the solution to air for 1 h. The solution was poured into a large amount of cold MeOH and the solid re-precipitated many times from cold THF/MeOH. The product was dried for 2 days at 40 °C under high vacuum to remove any residual solvent. For poly(S-*alt*-*p*HPMI): FTIR (KBr, cm^{-1}): 1705 (C═O), 3443 (O–H); ^{1}H NMR (500 MHz, DMSO-d_6, δ, ppm): 5.80–7.80 (m, 9H, Ar**H**), 9.71 (s, 1H, O**H**); ^{13}C NMR (125 MHz, DMSO-d_6, δ, ppm): 25.25 (C**H**$_2$CHCH), 30.85 (ArC**H**), 67.36 (CH$_2$C**H**CH), 79.11 (CH$_2$CHC**H**), 115.00–130.00 (Ar**C**), 157.28 (**C**OH), 176.30–179.30 (**C**═O). For poly(S-*alt*-*o*HPMI): FTIR (KBr, cm^{-1}): 1712 (C═O), 3435 (O–H); ^{1}H NMR (500 MHz, DMSO-d_6, δ, ppm): 5.80–7.80 (m, 9H, Ar**H**), 9.80 (s, 1H, O**H**); ^{13}C NMR (125 MHz, DMSO-d_6, δ, ppm): 25.25 (C**H**$_2$CHCH), 30.67 (ArC**H**), 67.01 (CH$_2$C**H**CH), 78.96 (CH$_2$CHC**H**), 116.00–131.00 (Ar**C**), 153.15 (**C**OH), 175.80–178.80 (**C**═O); Thermal decomposition temperatures (T_{d5} and T_{d10}) were 417 and 426 °C for poly(S-*alt*-*p*HPMI) (Figure S5), and 395 and 403 °C for poly(S-*alt*-*o*HPMI) (Figure S6).

2.5. Blend preparation

Blends of PVP with poly(S-*alt*-*p*HPMI) or poly(S-*alt*-*o*HPMI) were prepared through solution-casting (blend composition: 5 wt %). Each mixture was dissolved in DMF until the solution became homogeneous and then the solvent was evaporated over 2 days at 50 °C. The residual solvent was removed under high vacuum for 3 days at 90 °C.

2.6. Computational Details

All quantum chemical calculations were performed in the gas phase using the Gaussian 16 program [36]. The structures of *p*HPMI and *o*HPMI and their relative stability were investigated through geometry optimization, starting from different initial conformations of each molecule. Because copolymerizations with styrene involved reduction (saturation) of the maleimide CH═CH groups, calculations were also performed for *N*-(*p*-hydroxyphenyl)succinimide (*p*HPSI) and *N*-(*o*-hydroxyphenyl)succinimide (*o*HPSI). The difference in the glass transition temperatures (T_g) of poly(S-*alt*-*o*HPMI) and poly(S-*alt*-*p*HPMI) was investigated by modeling intermolecular interactions in the copolymers using dimers of *o*HPMI, *p*HPMI, *o*HPSI, and *p*HPSI. The interactions of the phenyl groups of the styrene moieties are much weaker than O–H···O hydrogen bonding [37–39] and contribute equally to the intermolecular interactions of both copolymers; thus, they were not considered. To gain insight into how the values of T_g of poly(S-*alt*-*p*HPMI) and poly(S-*alt*-*o*HPMI) changed when they were mixed with PVP, we also investigated the structures and interaction energies of the *N*-methyl-2-pyrrolidone (MP) dimer and complexes of MP with *o*HPSI and *p*HPSI. Calculations were performed with the density functional theory (DFT) using the B3LYP functional [40] and the 6-311G(d, p) basis set. Interaction energies of the homo and hetero dimers were calculated as the difference in energy between the complex and its interacting fragments Correction of interaction energies for basis set superposition error (BSSE) was performed using the counterpoise (CP) procedure of Boys and Bernardi [41]; both corrected (E^{CP}) and uncorrected (E) values are reported. To better describe dispersion-like interactions [42], complexation energies were also calculated with the M062X functional [43] using the geometries optimized with the B3LYP functional.

3. Results and discussion

3.1. Synthesis of HPMI monomers

We synthesized *p*HPMI and *o*HPMI by reacting maleic anhydride with 4-aminophenol and 2-aminophenol (Scheme 1). FTIR spectroscopy (Fig. 1) revealed that the narrow absorption band centered at 3482 cm^{-1} for the phenolic O–H stretching mode of *p*HPMI [Fig. 1(a)] shifted to a lower wavenumber (3377 cm^{-1}) and broadened for *o*HPMI [Fig. 1(b)], consistent with intramolecular hydrogen bonding in the latter between

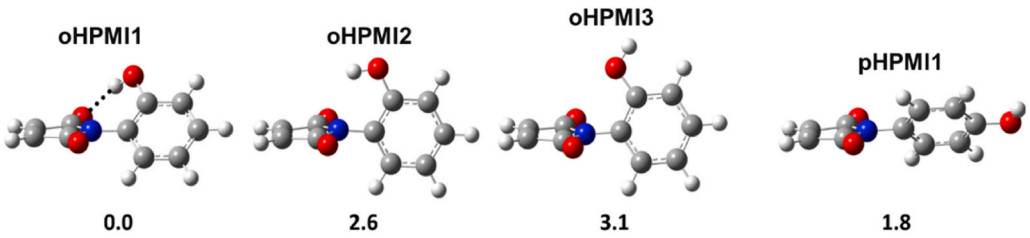

Fig. 2. Optimized geometries of *o*HPMI and *p*HPMI, calculated with B3LY/6-311g(d,p). Numbers show electronic energies relative to this of *o*HPMI1. Atom color code: H (white), C (gray), N (blue), and O (red). Dotted lines connect H-bonded atoms. Atomic coordinates are provided in the supporting information (SI). (For interpretation of the references to color in this figure legend, the reader is referred to the Web version of this article.)

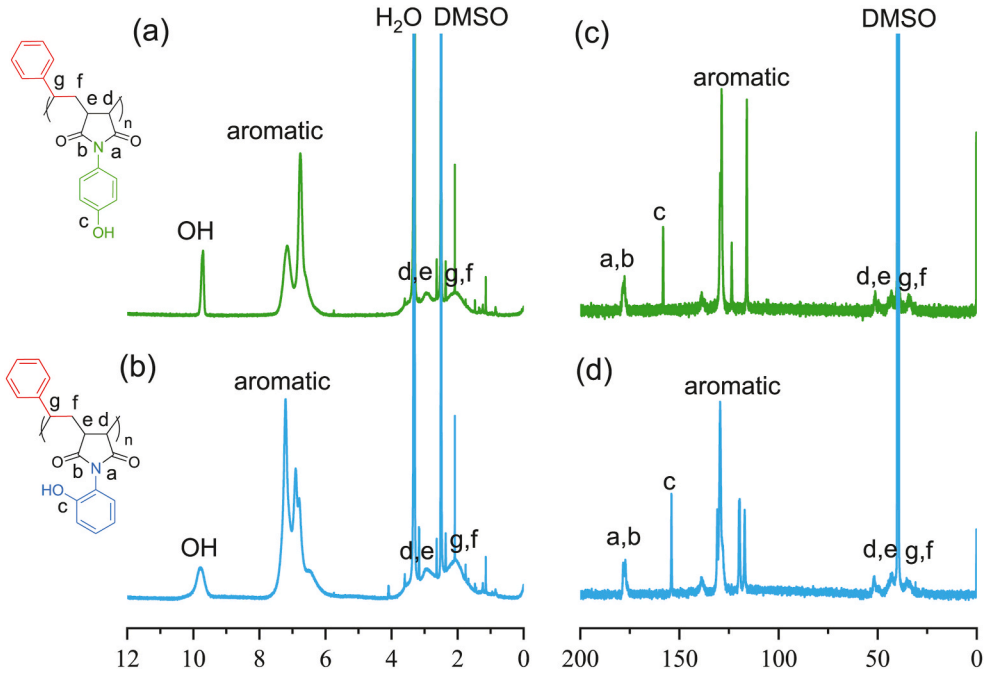

Fig. 3. ^{1}H and ^{13}C NMR spectra of (a, c) poly(S-*alt*-*p*HPMI) in DMSO-d_6 and (b, d) poly(S-*alt*-*o*HPMI) in DMSO-d_6.

the phenolic OH group and one of the C═O groups, as displayed by the scheme in Fig. 1(b).

We used quantum chemical simulations to examine the structures of these two HPMI isomers. Geometric optimization with B3LYP/6-311G (d,p) revealed three conformers for *o*HPMI and a single structure for *p*HPMI (Fig. 2). As expected, intramolecular O–H···O═C hydrogen bonding resulted in structure *o*HPMI1 being more stable than *o*HPMI2, *o*HPMI3, and *p*HPMI1, by 2.6, 3.1, and 1.8 kcal/mol, respectively. The *o*HPMI1 and *p*HPMI1 structures are characterized by interplanar angles of approximately 45°, compared with those of 70–85° for the other structures. Reduction of the maleimide moiety increases the electron density of its O atoms, thereby strengthening its hydrogen bonding and enhancing the stability of the *ortho* structure relative to the *para* structure. This difference in hydrogen bonding reflected the observation of different C═O bands in the FTIR spectra of *p*HPMI and *o*PHMI in Fig. 1 (c). The spectrum of *o*HPMI featured a broad absorption at a higher wavenumber (centered at 1712 cm^{-1}) with a shoulder at 1690-1660 cm^{-1}. In contrast, the signal for *p*HPMI was a singlet centered at 1705 cm^{-1}, indicative of homogeneous intermolecular hydrogen bonding displayed schematically in [Fig. 1(a)] between the *para* OH group and the C═O groups.

Figure S7 displays the ^{1}H and ^{13}C NMR spectra of these two HPMI monomers. The protons attached to the olefinic units of *p*HPMI and *o*HPMI appeared at 7.11 and 7.15 ppm, respectively, and the signals of their OH groups appeared at 9.72 [Fig. S7(a)] and 9.85 [Fig. S7(b)] ppm, respectively. Because of intramolecular hydrogen bonding, the signal of the OH group of *o*HPMI was shifted downfield relative to that of the OH group of *p*HPMI [44,45]. The ^{13}C NMR spectrum of *p*HPMI featured signals at 170.36, 157.06, and 134.56 ppm, representing the carbon nuclei of the C═O, COH, and olefinic units, respectively; for *o*HPMI, these signals appeared at 170.18, 154.00, and 135.00 ppm, respectively. All other protons and carbons are assigned in Figure S7. The FTIR and NMR spectral data confirmed that these two HPMI monomers were synthesized successfully.

3.2. Synthesis of PS-alt-PHPMI copolymers

The poly(S-*alt*-*p*HPMI) [Scheme 1(d)] and poly(S-*alt*-*o*HPMI) [Scheme 1(e)] copolymers were prepared through free radical copolymerization of styrene with the two HPMI monomers; FTIR and NMR spectroscopy and MALDI-TOF mass spectrometry confirmed their chemical structures. Figure S8 presents the FTIR spectra of poly(S-*alt*-*p*HPMI) and poly(S-*alt*-*o*HPMI) recorded at room temperature. The spectra of these two alternating copolymers were similar to those of the HPMI monomers, with strong signals for their OH and C═O groups, except that these two signals become broad after copolymerization with styrene, indicative of the presence of inter- and/or intramolecular hydrogen bonding [46,47]. Fig. 3 displays the ^{1}H and ^{13}C NMR spectra of these two alternating copolymers. Two broad peaks appeared in the ^{1}H NMR spectra between 1.43 and 3.72 ppm for these two copolymers,

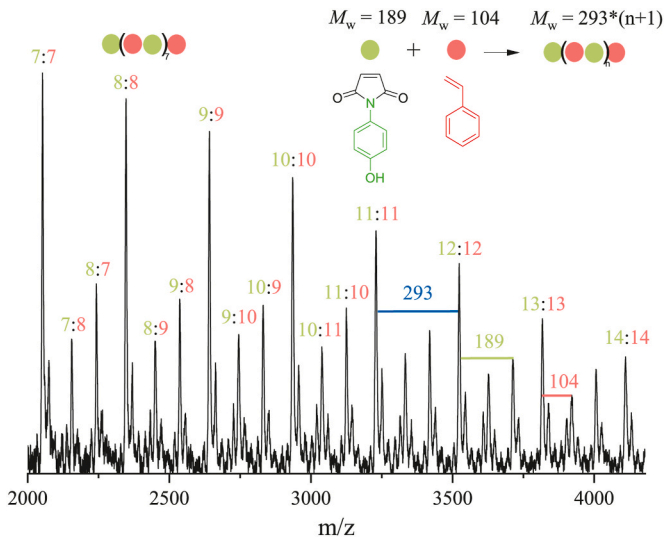

Fig. 4. MALDI-TOF mass spectrum of poly(S-*alt*-*p*HPMI) copolymer.

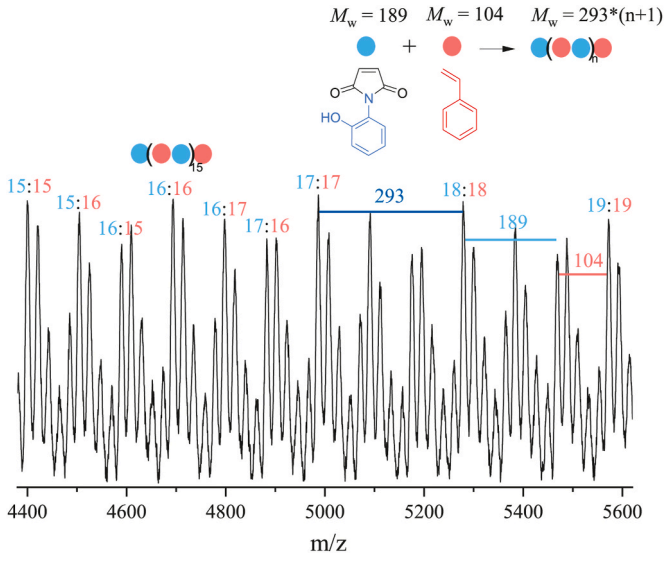

Fig. 5. MALDI-TOF mass spectrum of poly(S-*alt*-*o*HPMI) copolymer.

representing their main chain protons [Fig. 3(a) and (b)]; the signal of the phenolic OH groups was broader for poly(S-*alt*-*o*HPMI) than it was for poly(S-*alt*-*p*HPMI), again because of intramolecular hydrogen bonding between the *ortho* OH groups of the phenolic units and the C═O groups of the maleimide units. The ^{13}C NMR spectrum of poly (S-*alt*-*p*HPMI) featured signals at 176.30–179.30 and 157.28 ppm, representing the carbon nuclei of its C═O and COH groups, respectively; for poly(S-*alt*-*o*HPMI), they appeared at 175.80–178.80 and 153.15 ppm, respectively. All other protons and carbons are assigned in Fig. 3.

The styrene/HPMI monomer ratios in the alternating copolymers poly(S-*alt*-*p*HPMI) and poly(S-*alt*-*o*HPMI), calculated from the ^{1}H NMR spectra by integrating the signals of the OH groups and aromatic units, were 1/1.15 and 1/1.20, respectively. These values are consistent with alternating copolymers. Figs. 4 and 5 present the MALDI-TOF mass spectra of poly(S-*alt*-*p*HPMI) and poly(S-*alt*-*o*HPMI), respectively, revealing evidence for the copolymers having nearly perfect alternating individual chains with equal numbers of styrene and HPMI units [48, 49]. For example, the ~293 g mol^{-1} difference in the 2053.10 and 2346.71 *m/z* values in Fig. 4 for poly(S-*alt*-*p*HPMI) is equal to the summed molecular weights of one styrene and one *p*HPMI unit.

Table 1
The molecular weight and T_g behavior of poly(S-alt-*p*HPMI) and poly(S-alt-*o*HPMI) copolymer synthesized in this study.

Sample	M_n (g/mol)[a]	PDI[a]	T_g (°C)[b]
poly(S-alt-*p*HPMI)	2900	1.04	259
poly(S-alt-*o*HPMI)	4830	1.02	249

[a] by MALDI-TOF MS.
[b] by DSC.

Similarly, Fig. 5 provides a difference in the values of *m/z* of 4400.29 and 4693.62 for poly(S-*alt*-*o*HPMI) of ~293 g mol^{-1}. Furthermore, the intense peak at *m/z* 2346.71 in Fig. 4 corresponds to structures having eight units of styrene (8 × 104.15 u) and eight units of *p*HPMI (8 × 189.17 u) (labeled 8:8). The other intense peaks in the spectrum of poly (S-*alt*-*p*HPMI) correspond to perfectly alternating sequences having styrene:*p*HPMI ratios of *n*–1:*n*, *n*:*n*–1, and *n*:*n* (e.g., 8:9, 9:8, and 9:9, respectively) as displayed in Fig. 4 and Figure S9. Only a few weak peaks due to the styrene:*p*HPMI ratios of *n*–2:n and *n*+1:*n*-1 such as 7:9 and 10:8 because of homopolymerization of styrene and *p*HPMI. Based on the curve fitting result, the non-alternating segment was only 1.25% and thus we obtained the near-perfect alternating copolymer of poly(S-*alt*-*p*HPMI). The same phenomenon is evident in the spectrum of poly(S-*alt*-*o*HPMI) in Fig. 5, with an intense peak at *m/z* 4693.62 (labeled 16:16), corresponding to 16 units of styrene (16 × 104.15 u) and 16 units of *o*HPMI (16 × 189.17 u), as well as 16:17 and 17:16 distributions as also shown in Figure S10. Similarly, the few weak peaks due to the styrene:*o*HPMI ratios of *n*+2:*n*-1 and *n*:*n*+1 such as 17:15 and 16:18, due to the homopolymerization of styrene and *o*HPMI and only 0.92% non-alternating segment was calculated. Therefore, the MALDI-TOF mass spectra confirmed that we had obtained perfectly alternating copolymers of poly(S-*alt*-*p*HPMI) and poly(S-*alt*-*o*HPMI); Table 1 summarizes the molecular weights and polydispersities of these two alternating copolymers.

2.3. Analyses of PS-alt-PHPMI/PVP blends

Next, we examined the sequence distributions of these two alternating copolymers and their intermolecular hydrogen bonding interactions in polymer blend systems with the hydrogen-bond-accepting homopolymer PVP. DSC is a general method of thermal analysis for determining the miscibility of polymer blend systems; Fig. 6 displays the second-run DSC thermograms of various poly(S-*alt*-*p*HPMI)/PVP and poly(S-*alt*-*o*HPMI)/PVP blends. The pure poly(S-*alt*-*p*HPMI), poly(S-*alt*-*o*HPMI), and PVP had values of T_g of 259, 249, and 166 °C, respectively. The T_g value of the pure PVP homopolymer (166 °C) is similar to those determined previously [30–32]; poly(S-*alt*-*p*HPMI) and poly (S-*alt*-*o*HPMI) had values of T_g higher than those of other styrene-based copolymers featuring phenolic OH groups. For example, PS-*co*-PVPh copolymers containing various PVPh compositions have been reported to have T_g values of 100–180 °C [18]. Furthermore, an SMA copolymer having an MA composition of 50 wt% displayed a value of T_g of approximately 180 °C [50]. We suspect that poly(S-*alt*-*p*HPMI) and poly (S-*alt*-*o*HPMI) had higher T_g values than that of the SMA copolymer because the phenolic OH groups of our copolymers underwent strong intermolecular hydrogen bonding in their *p*HPMI and *o*HPMI units. Although the maleic anhydride monomer could not polymerize directly to form its homopolymer, if we take into account the glass transition temperature behavior of poly(S-*alt*-*p*HPMI) based on the Fox or linear rule [51], we expect a value of T_g for the poly(*p*HPMI) homopolymer close to 400 °C; it seems unlikely, however, that this homopolymer would have such a high value of T_g for this chemical structure. Therefore, we suspect that the alternating sequence distributions of our PS-*alt*-PHPMI copolymers played an important role in providing their high-T_g behavior. The PS diluent segments alternating with the HPMI segments would strongly inhibit self-association or intra-chain hydrogen

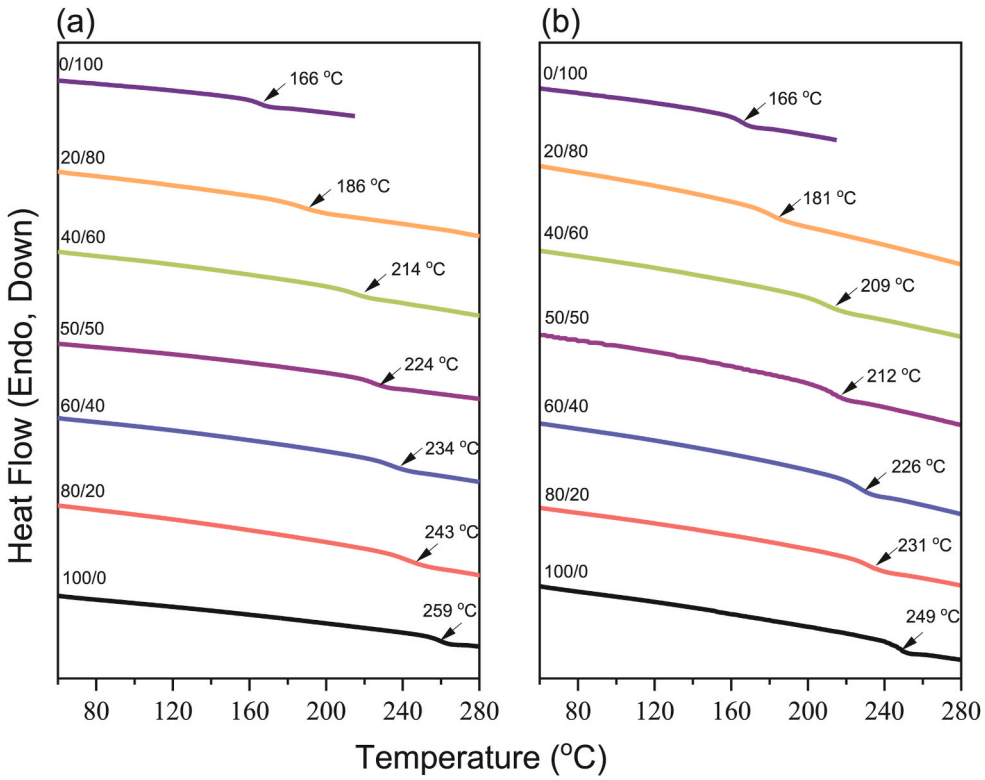

Fig. 6. DSC thermal analyses of (a) poly(S-*alt*-*p*HPMI)/PVP blends, (b) poly(S-*alt*-*o*HPMI)/PVP blends.

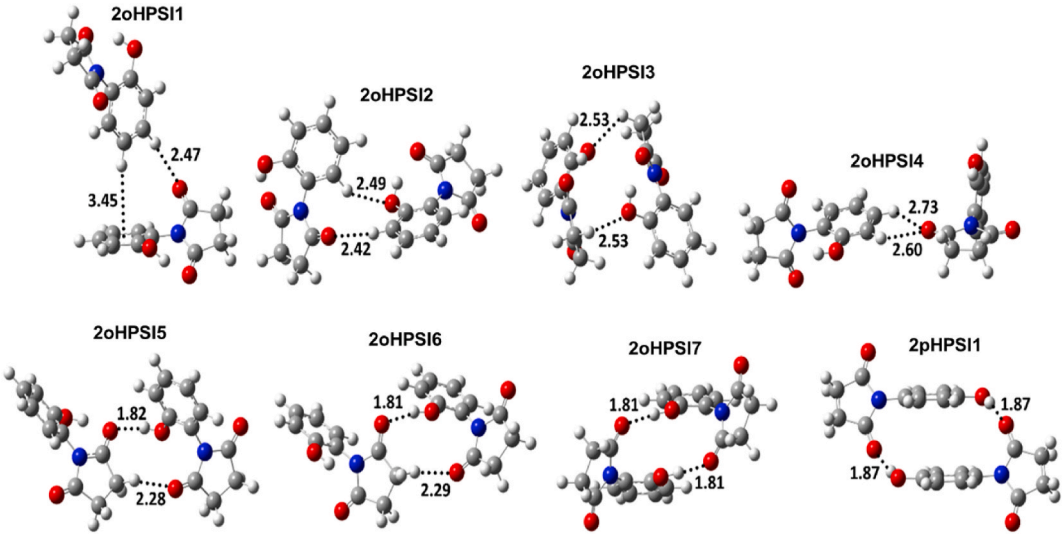

Fig. 7. Optimized energy-minimum conformers for dimers of *o*HPSI or *p*HPSI calculated with B3LY/6-311g(d,p).

bonding through OH···O interactions [24]; therefore, the possibility of inter-chain hydrogen bonding through OH···O interactions would increase, thereby decreasing the free volume and increasing the value of T_g significantly. We investigated the intermolecular interactions in poly (S-*alt*-*p*HPMI) and poly(S-*alt*-*o*HPMI) by considering the association of two *p*HPSI or *o*HPSI molecules.

Fig. 7 presents the optimized geometries of the *p*HPSI and *o*HPSI dimers and Table 2 lists their interaction energies calculated using the B3LYP and M062X density functionals. Figure S11 and Table S1 provide the corresponding structures and interaction energies of the related *p*HPMI and *o*HPMI dimers. The interaction energies predicted by M062X/6-311G(d,p) were larger (more negative values of E and E^{CP}) than those predicted by B3LYP/6-311G(d,p), presumably because of a better description of the dispersion forces when using the M062X functional. The calculations revealed seven structures of the ortho dimer and a single structure for the para dimer (Fig. 7 and S11). Interestingly, while the OH···O H-bonded conformer was the most stable structure of *o*HPSI (Fig. 2), dimers in which either or both monomers adopted this conformation (2*o*HPSI1-2*o*HPSI5) were of low stability (less negative interaction energies; Table 2), because a maximum of one strong intermolecular OH···O H-bond could form in these structures. In contrast, non-intramolecular hydrogen bonding in the interacting monomers of structure 2*o*HPSI7 resulted in two intermolecular OH···O═C bonds and, hence, the high stability of this structure. Although structure 2*o*HPSI7

Table 2
Interaction energy (E and E^{CP}, in kcal/mol) for the structures presented in Fig. 7.[a]

Structure	B3LYP/6-311G(d,p)		M062X/6-311G(d,p)[b]	
	E	E^{CP}	E	E^{CP}
2oHPSI1	−1.7	−0.7	−2.9	−2.1
2oHPSI2	−3.3	−1.5	−4.8	−3.3
2oHPSI3	−7.5	−4.5	−12.0	−9.5
2oHPSI4	−2.4	−1.1	−3.2	−2.2
2oHPSI5	−12.5	−9.2	−15.2	−12.4
2oHPSI6	−13.3	−9.9	−15.9	−13.1
2oHPSI7	−20.9	−15.9	−25.8	−21.6
2pHPSI1	−17.2	−13.0	−22.4	−18.8

[a] E and E^{CP} are interaction energies without and with correction for BSSE, respectively.
[b] Interaction energies are calculated on the geometries from B3LYP/6-311G (d,p) calculations.

was more stable than 2*p*HPSI1 by approximately 3 kcal/mol (E^{CP} values, Table 2), the other structures of the *ortho* dimer (2*o*HPSI1-2*o*HPSI6) were less stable than 2*p*HPSI1. Considering the three most stable structures of the *ortho* dimer (2*o*HPSI5-2*o*HPSI7), the average interaction energy (E^{CP}) was −11.7 kcal/mol; this value was 1.3 kcal/mol lower than that of the *para* dimer (2*p*HPSI1; $E^{CP} = -13\ 0$ kcal/mol). The higher value of T_g of poly(S-*alt*-*p*HPMI) (259 °C) relative to poly(S-*alt*-*o*HPMI) (249 °C) was, therefore, a consequence of stronger average intermolecular interactions in poly(S-*alt*-*p*HPMI). Notably, calculations of the *o*HPMI and *p*HPMI dimers yielded similar results (Figure S11, Table S1). For example, structure 2*o*HPMI7 was the most stable ortho structure and the *para* dimer (2*p*HPMI1) was on average more stable than the ortho one. Thus, stronger intermolecular hydrogen bonding occurred in the *para* dimer, but stronger intramolecular hydrogen bonding occurred in the *ortho* dimer, as expected.

Fig. 6 reveals a single value of T_g for all of the PS-*alt*-PHPMI/PVP blends, suggesting that these two blend systems possessed miscible behavior in the amorphous phase. Furthermore, the corresponding single values of T_g deviated largely and positively from the linear rule, as revealed in Fig. 8, suggesting that strong hydrogen bonding was likely in these two blend systems. The Kwei equation is generally used to describe the values of T_g of miscible blends featuring strong hydrogen bonding [52]:

$$T_g = \frac{W_1 T_{g1} + kW_2 T_{g2}}{W_1 + kW_2} + qW_1 W_2$$

where W_i represents the weight fraction of component *i*; T_{gi} is the glass transition temperature of component *i*; and k and q are fitting constants. After fitting the data to the Kwei equation (green lines), we obtained values of k and q of 1 and 45, respectively, for the poly(S-*alt*-*p*HPMI)/PVP blends and values of 1 and 30, respectively, for the poly(S-*alt*-*o*HPMI)/PVP blends. Thus, the poly(S-*alt*-*p*HPMI)/PVP blends displayed higher-T_g behavior at all blend compositions. For instance, the poly(S-*alt*-*p*HPMI)/PVP = 50/50 blend had a value of T_g of 224 °C, whereas the poly(S-*alt*-*o*HPMI)/PVP = 50/50 blend had a value of only 212 °C.

To examine the hydrogen bonding interactions in our poly(S-*alt*-*p*HPMI)/PVP and poly(S-*alt*-*o*HPMI)/PVP blend systems, we recorded their FTIR spectra (OH absorption regions) at 120 °C to avoid the absorption of moisture (Fig. 9). The spectrum of pure poly(S-*alt*-*p*HPMI) featured a broad OH stretching absorption, but that of pure poly(S-*alt*-*o*HPMI) had a relatively narrow signal. For the phenolic OH groups, the signals for free OH were located at 3550 cm^{-1} for both PS-*alt*-PHPMI copolymers; for the pure poly(S-*alt*-*p*HPMI) copolymer, a broad absorption appeared at 3445 cm^{-1}, whereas a relatively narrow absorption was centered at 3430 cm^{-1} for pure poly(S-*alt*-*o*HPMI), the result of the different distributions and rearrangements of their hydrogen-bonded units. In general, the centered position dominated for inter-association of OH···O=C units; thus, we assigned the signal at 3445 cm^{-1} to the intermolecular OH···O=C hydrogen bonding of pure poly(S-*alt*-*p*HPMI) and the signal at 3430 cm^{-1} to the intramolecular OH···O=C hydrogen bonding of pure poly(S-*alt*-*o*HPMI). Furthermore, the average hydrogen bonding strength can generally be determined from the frequency difference ($\Delta\nu$) between the signals for the free and hydrogen-bonded OH

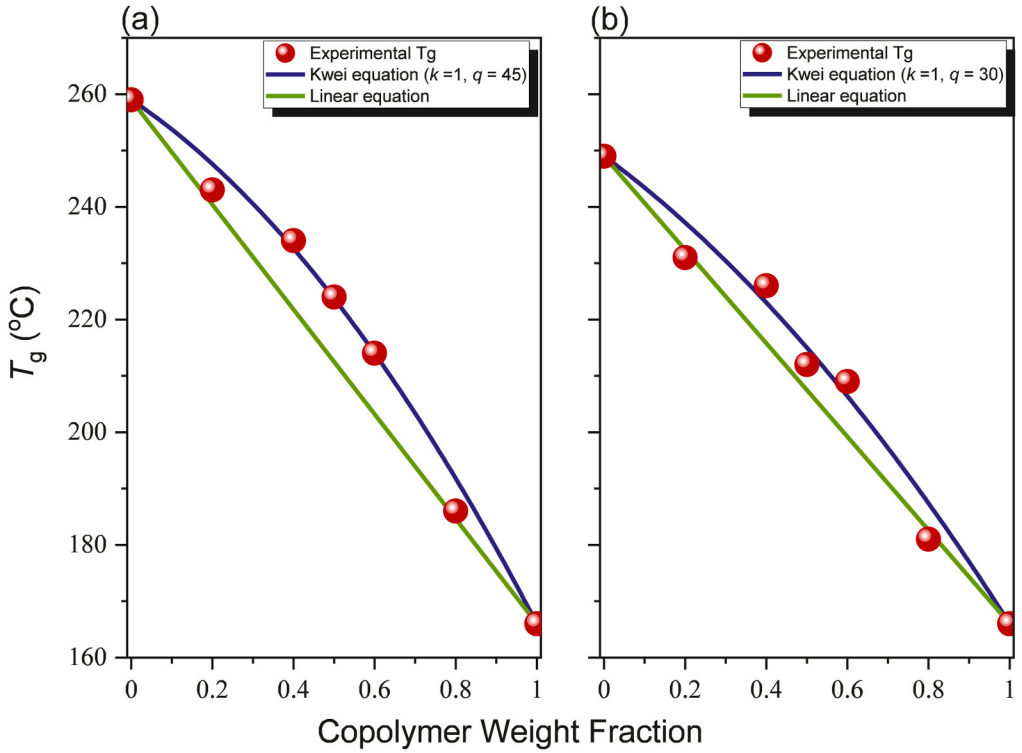

Fig. 8. Experimental T_g values with composition curves based on the Kwei equation for (a) poly(S-*alt*-*p*HPMI)/PVP blends and (b) poly(S-*alt*-*o*HPMI)/PVP blends.

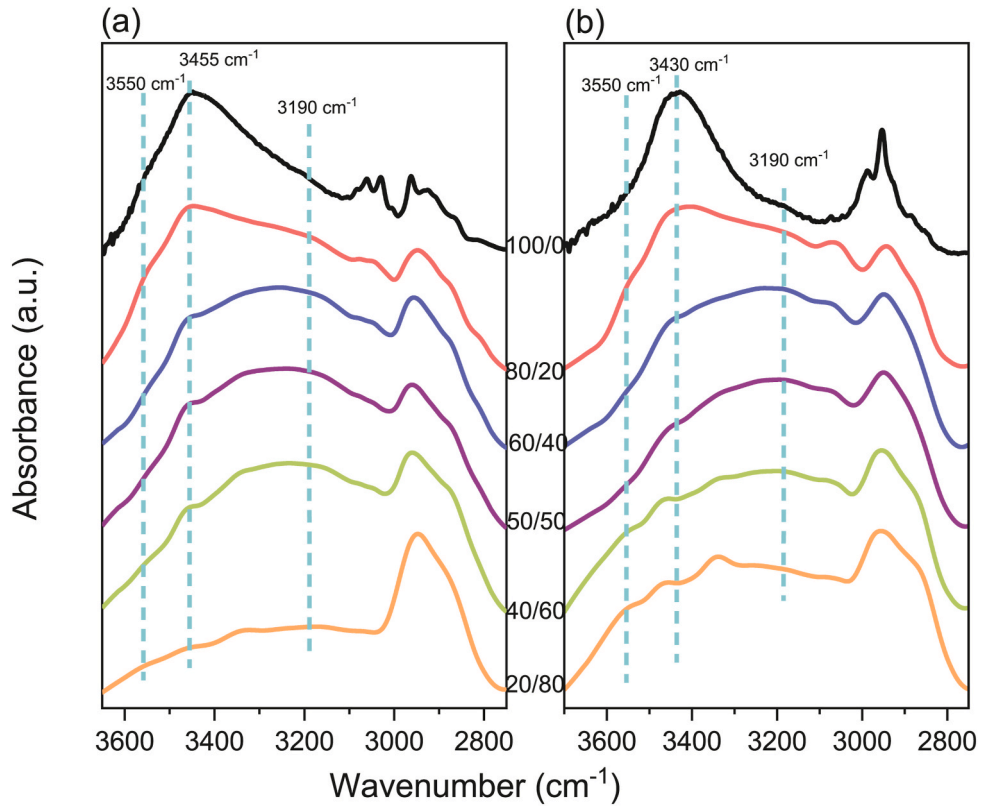

Fig. 9. FTIR spectra (2750–3650 cm^{-1}), recorded at 120 °C, for (a) poly(S-*alt*-*p*HPMI)/PVP and (b) poly(S-*alt*-*o*HPMI)/PVP blends.

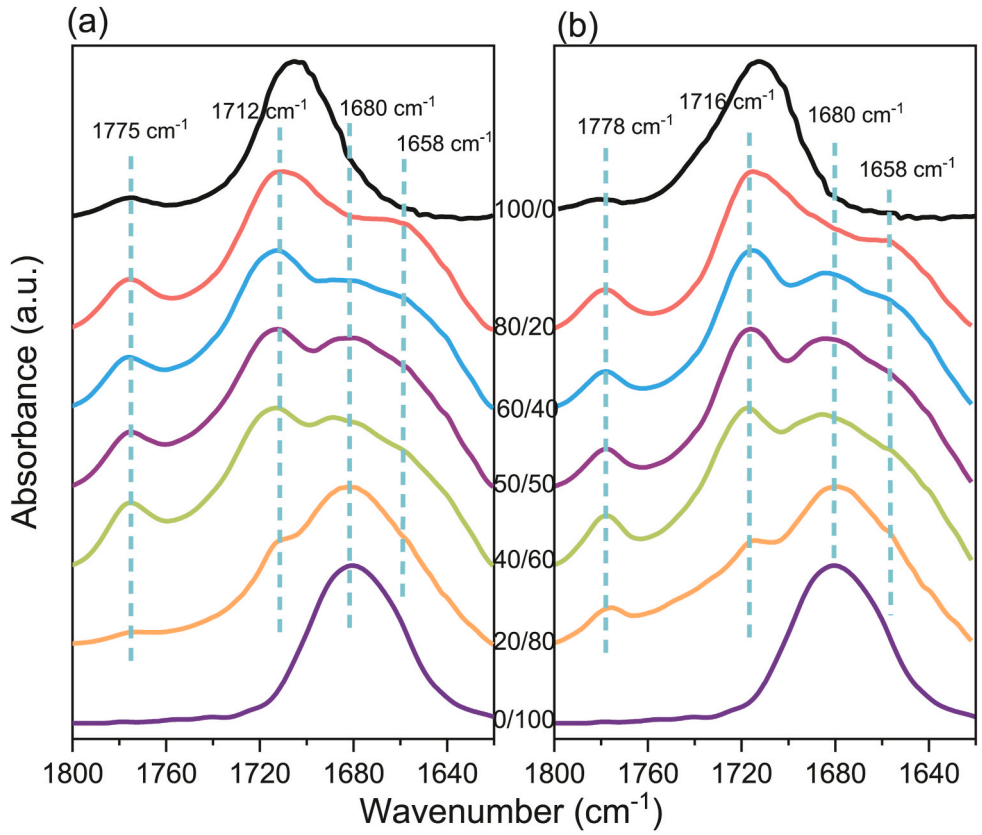

Fig. 10. FTIR spectra (1620–1800 cm^{-1}), recorded at 120 °C, for (a) poly(S-*alt*-*p*HPMI)/PVP blends, (b) poly(S-*alt*-*o*HPMI)/PVP blends.

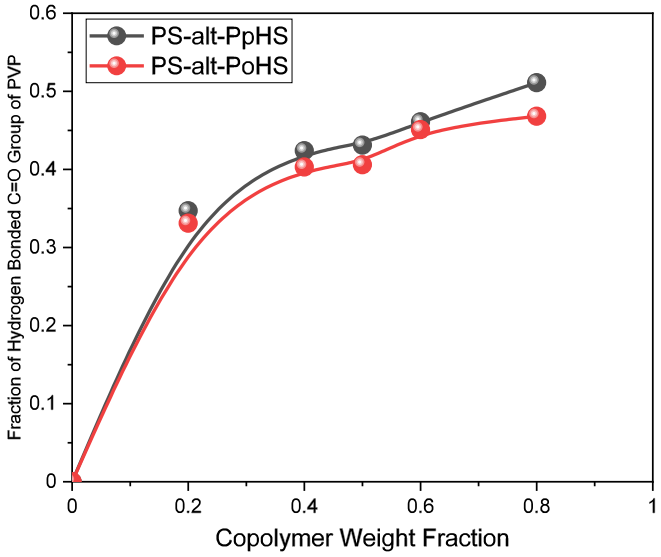

Fig. 11. Fraction of hydrogen bonded C═O group of PVP with copolymer weight fraction variation.

groups [47]; thus, we conclude that the intramolecular OH···O═C hydrogen bonding of the pure poly(S-*alt*-*o*HPMI) ($\Delta\nu$ = 120 cm^{-1}) was stronger than the intermolecular OH···O═C hydrogen bonding ($\Delta\nu$ = 105 cm^{-1}) of the pure poly(S-*alt*-*p*HPMI). Furthermore, these two bands were both shifted to 3190 cm^{-1}, a lower wavenumber, upon blending with 80 wt% of the PVP homopolymer, indicative of a switch from OH···O═C hydrogen bonding of the HPMI unit to inter-chain hydrogen bonding between the phenolic OH groups of the HPMI units and the C═O groups of the PVP. The shifts in the OH absorptions ($\Delta\nu$) of the poly (S-*alt*-*p*HPMI)/PVP and poly(S-*alt*-*p*HPMI)/PVP blends were 255 and 240 cm^{-1}, respectively. This finding is consistent with the positive values of *q* based on the Kwei equation, as well as the larger value of *q* of the poly(S-*alt*-*p*HPMI)/PVP blend relative to that of the poly (S-*alt*-*o*HPMI)/PVP blend.

Because the phenolic OH groups of *p*HPMI and *o*HPMI units would also interact with the C═O groups of PVP when forming miscible blends, we also observed significant wavenumber shifts for the signals of the

Table 3
Interaction energy (*E* and E^{CP}, in kcal/mol) for the structures presented in Fig. 12 [a].

Structure	B3LYP/6-311G(d,p)		**M062X/6–311G(d,p)**[b]	
	E	E^{CP}	E	E^{CP}
oHMP1	−2.8	−0.3	−6.6	−4.4
oHMP2	−2.0	−0.5	−3.6	−2.2
oHMP3	−3.1	−0.5	−6.5	−4.3
oHMP4	−3.9	−2.0	−4.9	−3.4
oHMP5	−6.8	−4.3	−10.3	−8.2
oHMP6	−7.1	−4.6	−11.0	−8.9
oHMP7	−9.5	−5.6	−14.6	−11.4
oHMP8	−9.5	−5.6	−15.6	−12.2
oHMP9	−14.8	−10.7	−19.7	−16.1
oHMP10	−15.5	−11.7	−18.1	−14.9
pHMP1	−3.8	−1.7	−6.5	−4.7
pHMP2	−4.8	−2.6	−6.3	−4.5
pHMP3	−12.7	−9.6	−14.3	−11.7
pHMP4	−13.3	−9.9	−15.1	−12.3

[a] *E* and E^{CP} are interaction energies without and with correction for BSSE, respectively.
[b] Interaction energies are calculated on the geometries from B3LYP/6-311G (d,p) calculations.

C═O groups of PVP (Fig. 10). The FTIR spectra of the two pure PS-*alt*-PHPMI copolymers both featured two signals for C═O absorptions, corresponding to asymmetric and symmetric MI units, at 1775–1778 and 1712-1716 cm^{-1}; the spectrum of the pure PVP homopolymer contained a single broad C═O signal at 1680 cm^{-1}. The latter was split into two bands at 1680 and 1658 cm^{-1} upon blending with the PS-*alt*-PHPMI copolymers, presumably representing the free and hydrogen-bonded C═O groups of PVP. Therefore, the four expected C═O signals were clearly evident for both PS-*alt*-PHPMI/PVP blends, and could be fitted well using Gaussian functions (Figure S12).

The fraction of hydrogen-bonded C═O groups of PVP increased upon increasing the content of the PS-*alt*-PHPMI copolymer; for each blend composition, the value for the poly(S-*alt*-*p*HPMI)/PVP blend was always higher than that for the poly(S-*alt*-*o*HPMI)/PVP blend (Fig. 11). We used quantum chemical simulations to investigate the intermolecular hydrogen bonding of these two PS-*alt*-PHPMI/PVP blend systems. Hu et al. proposed that strong dipole–dipole interactions and weak hydrogen bonding occur for pure PVP homopolymers [32].

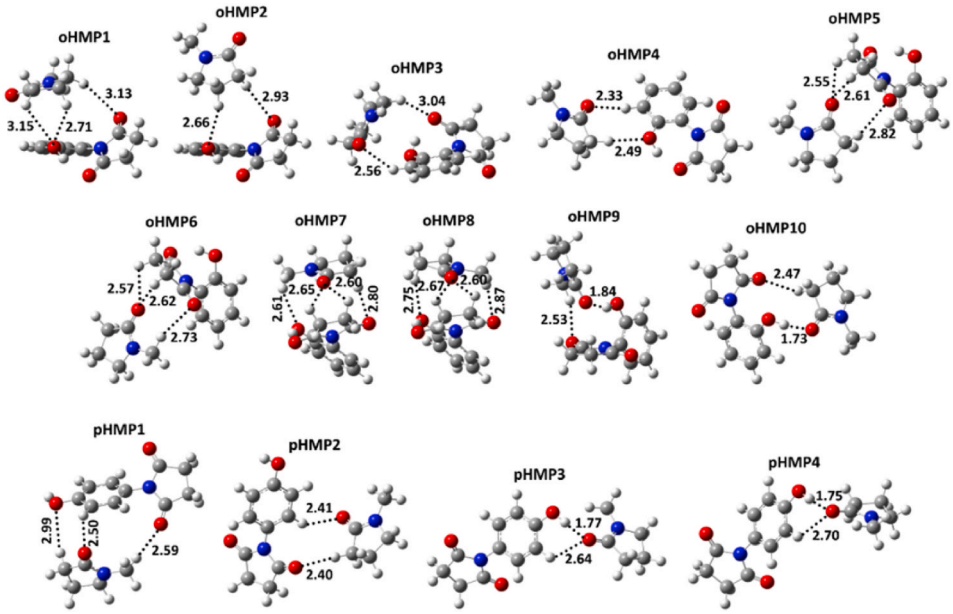

Fig. 12. Optimized energy-minimum conformers for the complexes of MP with *o*HPSI (*o*HMP) or *p*HPSI (*p*HMP) calculated with B3LY/6-311g(d,p).

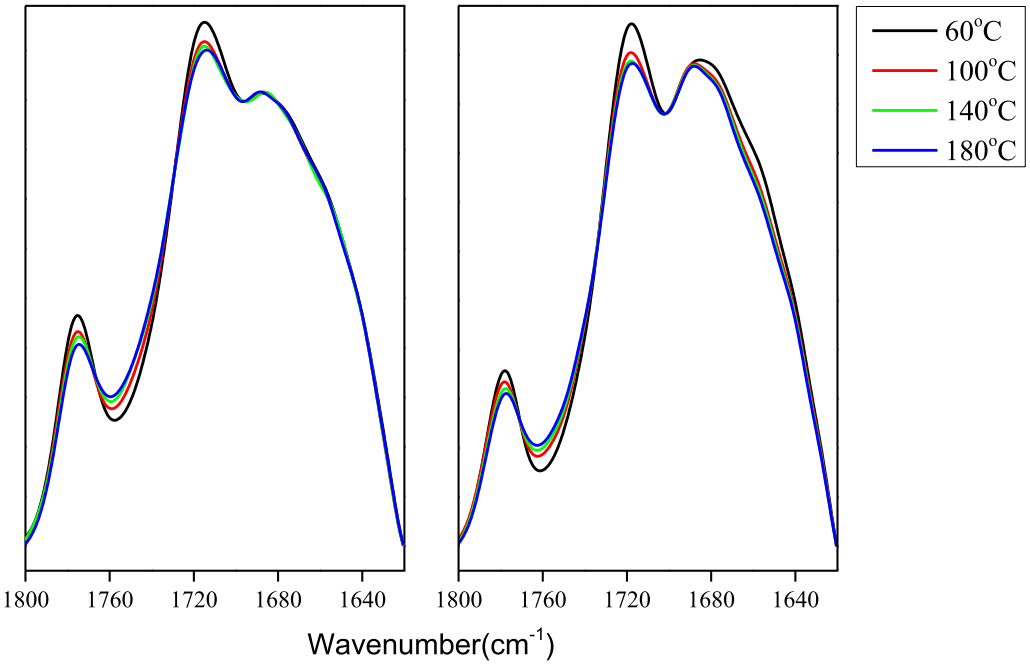

Fig. 13. FTIR spectra (1620–1800 cm^{-1}), recorded from 60 to 180 °C, for 40/60 ratio of (a) poly(S-*alt*-*p*HPMI)/PVP blends and (b) poly(S-*alt*-*o*HPMI)/PVP blends.

B3LYP/6-311G(d,p) calculations revealed seven stable structures for the MP dimer (Figure S13). Table S2 lists the interaction energies of these structures; again, the interaction energies from the M062X calculations were higher than those from the B3LYP calculations. Because of weak C–H···O═C hydrogen bonding (Figure S13), these structures had interaction energies ($E^{CP} \leq -3.1$ kcal/mol), lower than those of the most stable *p*HPSI and *o*HPSI dimers (*o*HPSI7: $E^{CP} = -15.9$ kcal/mol; pHPSI1: $E^{CP} = -13.0$ kcal/mol), which were stabilized by strong O–H···O═C hydrogen bonding (Fig. 7). To investigate the hydrogen bonding interactions of these two PS-*alt*-PHPMI/PVP blend systems at the molecular level, we modeled the interactions between the two polymers by using *p*HPSI/MP (*p*HMP) and *o*HPSI/MP (*o*HMP) pairs.

Fig. 12 displays the optimized structures of these complexes; Table 3 lists their interaction energies. Strong intermolecular O–H···O═C hydrogen bonding between MP and *p*HPSI or *o*HPSI resulted in structures *o*HMP9, *o*HMP10, *p*HMP3, and *p*HMP4 being more stable than structure 2MP7. Although these binary complexes were less stable than the *p*HPSI or *o*HPSI dimers (2*o*HPSI7 and 2*p*HPSI1), intermolecular hydrogen bonding still occurred because the value of K_A between a phenolic OH group and a C═O group of PVP is 6000—much stronger than the values of K_B for OH···OH (66.8) hydrogen bonding and the OH···O═C (67.4) interactions of typical acrylates or esters [51]. Because the values of K_A would be similar for the poly(S-*alt*-*p*HPMI)/PVP and poly(S-*alt*-*o*HPMI)/PVP blends, the value of K_B of poly(S-*alt*-*o*HPMI) would be higher than that of poly(S-*alt*-*p*HPMI) because of the extra intramolecular OH···O═C hydrogen bonding of the former's *o*HPMI units. As a result, the K_A/K_B ratio of the poly(S-*alt*-*o*HPMI)/PVP blends would decrease; thus, the average hydrogen bonding strength and fraction of hydrogen-bonded C═O groups of PVP both were lower when compared with those of the poly(S-*alt*-*p*HPMI)/PVP blends. To confirm the different hydrogen bonding strengths in these two-blend systems, we examined whether the intermolecular interactions between these alternating copolymers and PVP were influenced by the temperature (Fig. 13). For the poly(S-*alt*-*p*HPMI)/PVP blends, the fraction of hydrogen-bonded C═O groups of PVP remained almost unchanged upon increasing the temperature; in contrast, for the poly(S-*alt*-*o*HPMI)/PVP blends, this fraction decreased accordingly, indicative of stable intermolecular hydrogen bonding in the poly(S-*alt*-*p*HPMI)/PVP blends.

4. Conclusions

We synthesized two isomeric HPMI monomers, featuring *para* and *ortho* phenolic OH groups, and then formed poly(S-*alt*-*p*HPMI) and poly(S-*alt*-*o*HPMI) alternating copolymers through free radical copolymerizations with styrene. The structures of the copolymers were characterized using FTIR and NMR spectroscopy and MALDI-TOF mass spectrometry. DSC analyses revealed that both sets of PS-*alt*-PHPMI/PVP blends had a single value of T_g at each blend composition, indicating full miscibility in the amorphous phase, arising from strong intermolecular hydrogen bonding between the OH groups of PHPMI and the C═O groups of PVP, as evidenced through FTIR spectral analyses and quantum chemical calculations. Because the *ortho* OH groups of the phenolic units of *o*HPMI could also experience intramolecular hydrogen bonding with the C═O groups of their maleimide units, their intermolecular interactions were weaker than those of the para OH groups of the phenolic units of *p*HPMI. As a result, the K_A/K_B ratio of the poly(S-*alt*-*o*HPMI)/PVP blends was low and, therefore, the average hydrogen bonding strength, the fraction of hydrogen-bonded C═O groups of PVP, and the values of T_g were all lower relative to those of the poly(S-*alt*-*p*HPMI)/PVP blends.

CRediT authorship contribution statement

Wei-Ting Du: Methodology, Synthesis, Investigation, Formal analysis, Writing - original draft. **Esam A. Orabi:** Investigation, Formal analysis, Writing - original draft. **Mohamed Gamal Mohamed:** Synthesis, Investigation. **Shiao-Wei Kuo:** Supervision, Writing - original draft, Writing - review & editing.

Declaration of competing interest

The authors declare that they have no known competing financial interests or personal relationships that could have appeared to influence the work reported in this paper

Acknowledgments

This study was supported financially by the Ministry of Science and

Technology, Taiwan, under contracts MOST108-2638-E-002-003-MY2, and 108-2221-E-110-014-MY3.

Appendix A. Supplementary data

Supplementary data to this article can be found online at https://doi.org/10.1016/j.polymer.2021.123542.

References

[1] H. Wang, X. Yang, Z. Fu, X. Zhao, Y. Li, J. Li, Rheology of nanosilica-compatibilized immiscible polymer blends: formation of a "heterogeneous network" facilitated by interfacially anchored hybrid nanosilica, Macromolecules 50 (2017) 9494–9506.

[2] I. Charfeddine, J.C. Majeste, C. Carrot, O. Lhost, A model for the prediction of the morphology of immiscible blends of polymers, Polymer 193 (2020) 122334.

[3] J. Wang, A.H. Tsou, B.D. Favid, Effects of polyethylene molecular weight distribution on phase morphology development in poly(p-phenylene ether) and polyethylene blends, Macromolecules 51 (2018) 9165–9176.

[4] D. Bruns, T.E. de Oliveira, J. Rottler, D. Mukherji, Tuning morphology and thermal transport of asymmetric smart polymer blends by macromolecular engineering, Macromolecules 52 (2019) 5510–5517.

[5] B.H. Mao, A.F.M. EL-Mahdy, S.W. Kuo, Bio-inspired multiple complementary hydrogen bonds enhance the miscibility of conjugated polymers blended with polystyrene derivatives, J. Polym. Res. 26 (2019) 208.

[6] C.T. Tsou, S.W. Kuo, Competing hydrogen bonding interaction creates hierarchically ordered self-assembled structures of PMMA-b-P4VP/PVPh-b-PS mixtures, Macromolecules 52 (2019) 8374–8383.

[7] D. Prusty, V. Pryamitsyn, M.O. de la Cruz, Thermodynamics of associative polymer blends, Macromolecules 51 (2018) 5918–5932.

[8] Y.S. Lu, Y.C. Lin, S.W. Kuo, Separated coil and chain aggregation behaviors on the miscibility and helical peptide secondary structure of poly(tyrosine) with poly(4-vinylpyridine), Macromolecules 45 (2012) 6547–6556.

[9] M.M. Coleman, J.F. Graf, P.C. Painter, Specific Interactions and the Miscibility of Polymer Blends, Technomic Publishing, Lancaster, PA, 1991.

[10] M.M. Coleman, P.C. Painter, Hydrogen bonded polymer blends, Prog. Polym. Sci. 20 (1995) 1–59.

[11] M.M. Coleman, P.C. Painter, Miscible Polymer Blends: Background and Guide for Calculations and Design, DEStech Publication Inc., Lancaster, PA, 2006.

[12] P.C. Painter, M.M. Coleman, in: D.R. Paul, C.B. Bucknall (Eds.), Hydrogen Bonding Systems in Polymer Blends, Wiley, New York, 2000, pp. 93–140.

[13] M. Jiang, L. Mei, M. Xiang, H. Zhou, Interpolymer complexation and miscibility enhancement by hydrogen bonding, Adv. Polym. Sci. 146 (1999) 121–196.

[14] Y. He, B. Zhu, Y. Inoue, Hydrogen bonds in polymer blends, Prog. Polym. Sci. 29 (2004) 1021–1051.

[15] A. Prinos, A. Dompros, C. Panayiotou, Thermoanalytical and spectroscopic study of poly (vinyl pyrrolidone)/poly (styrene-co-vinyl phenol) blends, Polymer 39 (1998) 3011–3016.

[16] J.Q. Zhao, E.M. Pearce, T.K. Kwei, Binary and ternary blends of polystyrene-block-poly(p-hydroxystyrene), Macromolecules 30 (1997) 7119–7126.

[17] S.W. Kuo, C.F. Huang, P.H. Tung, W.J. Huang, J.M. Huang, F.C. Chang, Synthesis, thermal properties and specific interactions of high T_g increase in poly(2,6-dimethyl-1,4-phenylene oxide)-block-Polystyrene copolymers, Polymer 46 (2005) 9348–9361.

[18] S.W. Kuo, F.C. Chang, Effects of copolymer composition and free volume change on the miscibility of poly(styrene-co-vinylphenol) with poly(ε-caprolactone), Macromolecules 34 (2001) 7737–7743.

[19] S.W. Kuo, F.C. Chang, Effect of copolymer composition on the miscibility of poly (styrene-co-acetoxystyrene) with phenolic resin, Polymer 42 (2001) 9843–9848.

[20] Y. Xu, P.C. Painter, M.M. Coleman, Synthesis and infra-red spectroscopic characterization of random copolymers of 4-vinylphenol with n-alkyl methacrylates, Polymer 34 (1993) 3010–3018.

[21] C.L. Lin, W.C. Chen, C.S. Liao, Y.C. Su, C.F. Huang, S.W. Kuo, F.C. Chang, Sequence distribution and polydispersity index affect the hydrogen-bonding strength of poly (vinylphenol-co-methyl methacrylate) copolymers, Macromolecules 38 (2005) 6435–6444.

[22] T.C. Tseng, S.W. Kuo, Hydrogen-bonding strength influences hierarchical self-assembled structures in unusual miscible/immiscible diblock copolymer blends, Macromolecules 51 (2018) 6451–6459.

[23] M.G. Mohamed, Y.R. Jheng, S.W. Kuo, Unusual emission of polystyrene-based alternating copolymers incorporating aminobutyl maleimide fluorophore-containing polyhedral oligomeric silsesquioxane nanoparticles, Polymers 9 (2017) 103.

[24] S.W. Kuo, F.C. Chang, Effect of inert diluent segment on the miscibility behavior of poly(vinylphenol) with poly(acetoxystyrene) blends, J. Polym. Sci., Part B: Polym. Phys. 40 (2002) 1661–1672.

[25] G. Li, J.M.G. Cowie, V. Arrighi, Miscibility of polymer blends of poly(styrene-co-4-hydroxystyrene) with bisphenol-A polycarbonate, J. Appl. Polym. Sci. 74 (1999) 639–646.

[26] G.D. Merfeld, D.R. Paul, in: D.R. Paul, C.B. Bucknall (Eds.), Polymer–polymer Interactions Based on Mean Field Approximations in Polymer Blends, Wiley, New York, 2000, pp. 55–92.

[27] G. Odian, Principles of Polymerization, Wiley, New York, 2004.

[28] D. Mathew, C.P. Nair, K.N. Ninan, Pendant cyanate functional vinyl polymers and imido-phenolic-triazines thereof: synthesis and thermal properties, Eur. Polym. J. 36 (2000) 1195–1208.

[29] K. Izu, Y. Tokoro, T. Oyama, Simultaneous improvement of mechanical properties and curing temperature of cyanate ester resin by in situ generated modifier polymer having phenolic OH group, Polymer 202 (2020) 122611.

[30] S.W. Kuo, F.C. Chang, Studies of miscibility behavior and hydrogen bonding in blends of poly(vinylphenol) and poly(vinylpyrrolidone), Macromolecules 34 (2001) 5224–5228.

[31] W.C. Chen, S.W. Kuo, U.S. Jeng, F.C. Chang, Self-assembly through competitive interactions of miscible diblock copolymer/homopolymer blends: poly(vinyl phenol-b-methyl meth acrylate)/Poly(vinylpyrrolidone) blend, Macromolecules 41 (2008) 1401–1410.

[32] Y. Hu, H.R. Motzer, A.M. Etxeberria, M.J. Fernadez-Berridi, J.J. Iruin, P.C. Painter, M.M. Coleman, Concerning the self-association of N-vinyl pyrrolidone and its effect on the determination of equilibrium constants and the thermodynamics of mixing, Macromol. Chem. Phys. 201 (2000) 705–714.

[33] K. Zhang, X. Yu, S.W. Kuo, Outstanding dielectric and thermal properties of main chain-type poly (benzoxazine-co-imide-co-siloxane)-based cross-linked networks, Polym. Chem. 10 (2019) 2387–2396.

[34] K. Zhang, J. Liu, H. Ishida, An ultrahigh performance cross-linked polybenzoxazole via thermal conversion from poly(benzoxazine amic acid) based on smart o-benzoxazine chemistry, Macromolecules 47 24 (2014) 8674–8681.

[35] W.C. Chen, S.W. Kuo, Ortho-Imide and allyl groups effect on highly thermally stable polybenzoxazine/double-decker-shaped polyhedral silsesquioxane hybrids, Macromolecules 51 (2018) 9602–9612.

[36] M.J. Frisch, G.W. Trucks, H.B. Schlegel, G.E. Scuseria, M.A. Robb, J.R. Cheeseman, G. Scalmani, V. Barone, G.A. Petersson, H. Nakatsuji, X. Li, M. Caricato, A. V. Marenich, J. Bloino, B.G. Janesko, R. Gomperts, B. Mennucci, H.P. Hratchian, J. V. Ortiz, A.F. Izmaylov, J.L. Sonnenberg, D. Williams-Young, F. Ding, F. Lipparini, F. Egidi, J. Goings, B. Peng, A. Petrone, T. Henderson, D. Ranasinghe, V. G. Zakrzewski, J. Gao, N. Rega, G. Zheng, W. Liang, M. Hada, M. Ehara, K. Toyota, R. Fukuda, J. Hasegawa, M. Ishida, T. Nakajima, Y. Honda, O. Kitao, H. Nakai, T. Vreven, K. Throssell, J.A. Montgomery Jr., J.E. Peralta, F. Ogliaro, M. J. Bearpark, J.J. Heyd, E.N. Brothers, K.N. Kudin, V.N. Staroverov, T.A. Keith, R. Kobayashi, J. Normand, K. Raghavachari, A.P. Rendell, J.C. Burant, S.S. Iyengar, J. Tomasi, M. Cossi, J.M. Millam, M. Klene, C. Adamo, R. Cammi, J.W. Ochterski, R.L. Martin, K. Morokuma, O. Farkas, J.B. Foresman, D.J. Fox, Gaussian 16, Revision A.03, Gaussian, Inc., Wallingford CT, 2016.

[37] E.A. Orabi, G. Lamoureux, Cation−π and π−π interactions in aqueous solution studied using polarizable potential models, J. Chem. Theor. Comput. 8 (2012) 182–193.

[38] E.A. Orabi, R.L. Davis, G. Lamoureux, Drude polarizable force field for cation–π interactions of alkali and quaternary ammonium ions with aromatic amino acid side chains, J. Comput. Chem. 41 (2020) 472–481.

[39] E.A. Orabi, J.D. Faraldo-Gomez, New molecular-mechanics model for simulations of hydrogen fluoride in chemistry and biology, J. Chem. Theor. Comput. 16 (2020) 5105–5126.

[40] P.J. Stephens, F.J. Devlin, C.F. Chabalowski, M.J. Frisch, Ab initio calculation of Vibrational absorption and circular dichroism spectra using density functional force fields, J. Phys. Chem. 98 (1994) 11623–11627.

[41] S.F. Boys, F. Bernardi, The calculation of small molecular interactions by the differences of separate total energies. Some procedures with reduced errors, Mol. Phys. 19 (1970) 553–566.

[42] E.A. Orabi, Tautomerism and antioxidant activity of some 4-acylpyrazolone-based schiff bases: a theoretical study, RSC Adv. 8 (2018) 30842–30850.

[43] Y. Zhao, D.G. Truhlar, The M06 suite of density functionals for main group thermochemistry, thermochemical kinetics, noncovalent interactions, excited states, and transition elements: two new functionals and systematic testing of four M06-class functionals and 12 other functionals, Theor. Chem. Acc. 120 (2008) 215–241.

[44] P. Dhanishta, P.S. Kumar, S.K. Mishra, N. Suryaprakash, Intramolecular hydrogen bond directed stable conformations of benzoyl phenyl oxalamides: unambiguous evidence from extensive NMR studies and DFT-based computations, RSC Adv. 8 (2018) 11230–11240.

[45] S. Zhou, L. Wang, Symmetry and ^{1}H NMR chemical shifts of short hydrogen bonds: impact of electronic and nuclear quantum effects, Phys. Chem. Chem. Phys. 22 (2020) 4884–4895.

[46] W.C. Chen, R.C. Lin, S.M. Tseng, S.W. Kuo, Minimizing the strong screening effect of polyhedral oligomeric silsesquioxane nanoparticles in hydrogen-bonded random copolymers, Polymers 10 (2018) 303.

[47] C.W. Chiou, Y.C. Lin, L. Wang, C. Hirano, Y. Suzuki, T. Hayakawa, S.W. Kuo, Strong screening effect of polyhedral oligomeric silsesquioxanes (POSS) nanoparticles on hydrogen bonded polymer blends, Polymers 6 (2014) 926–948.

[48] M.G. Mohamed, K.C. Hsu, J.L. Hong, S.W. Kuo, Unexpected fluorescence from maleimide-containing polyhedral oligomeric silsesquioxanes: nanoparticle and sequence distribution analyses of polystyrene-based alternating copolymer, Polym. Chem. 7 (2016) 135–145.

[49] L.R. Hutchings, P.P. Brooks, D. Parker, J.A. Mosely, S. Sevinc, Monomer sequence control via living anionic copolymerization: synthesis of alternating, statistical, and telechelic copolymers and sequence analysis by MALDI ToF mass spectrometry, Macromolecules 48 (2015) 610–628.

[50] J.J. Benvenuta-Tapia, E. Vivaldo-Lima, T. Tenorio-Lopez, M. Vargas-Hernandez, H. Vazquez-Torres, Kinetic analysis of the RAFT copolymerization of styrene and

maleic anhydride by differential scanning calorimetry, Thermochim. Acta 667 (2018) 93–101.
[51] S.W. Kuo, Hydrogen Bonding in Polymeric Materials, John Wiley & Sons, 2018.
[52] T. Kwei, The effect of hydrogen bonding on the glass transition temperatures of polymer mixtures, J. Polym. Sci. Polym. Lett. Ed. 22 (1984) 307–313.